



Taguchi-Based Optimization of Air-Gap Membrane Distillat

Jasurjon Akhatov¹, Murodbek Kuralov*¹, Akbar Halimov¹,
Abdurauf Usmanov¹ and
Tukhtamurod Juraev¹

Technical Institute of the Uzbekistan Academy of Sciences, 2B, Chingiz Aytmatov str.,
Tashkent, 100084, Uzbekistan
makuralov@gmail.com

Abstract. This study investigates the performance optimization of an air-gap membrane distillation (AGMD) system using Taguchi-based orthogonal experimental design (OED). Four key operational parameters feed temperature (T_1), coolant temperature (T_2), feed flow rate (V_1), and coolant flow rate (V_2) were examined at two levels each, following an L_8 fractional factorial array. Three performance indicators were evaluated: permeate flux, distillate mass, and product conductivity. Experiments were conducted under steady-state conditions with T_1 at 70 and 80 °C, T_2 at 20/25 °C, and flow rates between 100–150 L/h. Results showed permeate flux ranging from 36.72 to 122.11 L/h, distillate mass from 0.158 to 1.328 kg, and conductivity from 1.23 to 3.69 $\mu\text{S cm}^{-1}$. Taguchi analysis identified feed temperature (T_1) as the most influential factor, contributing 56.4% to flux variation and 69.8% to distillate mass. Contrary to conventional expectations, raising T_1 from 70 °C to 80 °C reduced both flux and yield by over 60%, likely due to boundary-layer polarization and partial membrane wetting. Conductivity increased with higher T_1 and T_2 but was unaffected by V_1 , suggesting temperature-driven membrane integrity loss. The optimal trade-off—maximizing flux 118 L/h while maintaining high product quality 1.3 $\mu\text{S cm}^{-1}$ was achieved at $T_1 = 70$ °C, $T_2 = 20$ °C, $V_1 = 150$ L/h, and $V_2 = 100$ L/h. The OED approach cut experimental effort by 50% versus full factorial design, demonstrating its efficiency and reliability for optimizing AGMD systems powered by low-grade or renewable thermal energy.

Keywords: Air-gap membrane distillation, orthogonal experimental design, Taguchi method, permeate, distillate, thermal desalination.

1 Introduction

Global water scarcity affects more than 2.3 billion people across 48 countries, with projections indicating that by 2025, two-thirds of the world's population could face water-stressed conditions [1]. Desalination is increasingly seen as a critical mitigation strategy, with global installed capacity exceeding 100 million m^3/day in 2023, dominated by energy-intensive thermal and reverse osmosis processes [2]. In this context,

membrane distillation (MD), a thermally driven separation process—offers a compelling alternative due to its ability to operate efficiently at low feed temperatures 40–80 °C, enabling integration with solar collectors, geothermal sources, or industrial waste heat [3], [4]. A simplified schematic of the MD transport mechanism is shown in **figure 1**.

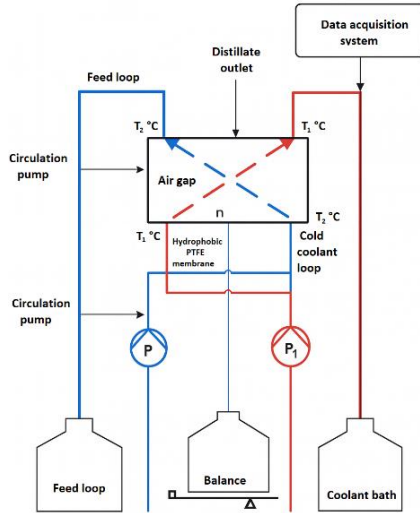


Fig. 1. Schematic representation of the operating principle of membrane distillation

Among MD configurations, air-gap membrane distillation is particularly attractive, achieving product conductivity below $10 \mu\text{S cm}^{-1}$ and thermal efficiency up to 70% in laboratory-scale studies [5].

However, AGMD performance remains highly sensitive to operational parameters. Permeate flux—the primary productivity indicator—can vary by over 200% with modest changes in feed temperature alone. For instance, increasing feed temperature from 50 °C to 70 °C has been reported to raise flux from 20 to 60 $\text{L m}^{-2} \text{h}^{-1}$ [6], yet further elevation to 80 °C or higher often leads to flux decline or instability due to membrane wetting or severe temperature polarization [7]. Similarly, coolant temperature directly influences the vapor pressure gradient across the membrane; reducing coolant temperature from 25 °C to 15 °C can increase flux by 15–25%, but at the cost of higher pumping energy and system complexity [8].

To systematically navigate these trade-offs, experimental optimization is essential. Full factorial design for four factors at two levels would require 16 experiments, but the Taguchi method reduces this to just 8 runs using an L_8 orthogonal array, cutting experimental time and resource use by 50% while preserving statistical reliability [5]. This efficiency is critical for early-stage process development, especially in resource-limited settings. Recent studies confirm Taguchi's effectiveness in MD: Khalifa & Lawal [6] reported a maximum AGMD flux of $76.0 \text{ L m}^{-2} \text{h}^{-1}$ using Taguchi-optimized conditions, while another study achieved a distillate conductivity as low as $1.2 \mu\text{S cm}^{-1}$ under similar design frameworks [3].

Despite these advances, few studies simultaneously evaluate multiple performance metrics—flux, total distillate mass, and product conductivity—under statistically robust designs. Most focus solely on flux maximization, potentially overlooking compromises in product quality or long-term stability. For example, high feed flow rates >150 L/h may boost flux by 20% through reduced concentration polarization, but can increase energy consumption without improving water quality [9]. Conversely, low coolant flow rates <100 L/h might enhance condensation residence time and total yield but risk condensate flooding in the air gap [10].

This study addresses these gaps by applying Taguchi-based orthogonal experimental design to a lab-scale AGMD system to quantitatively assess the relative influence of four key parameters—feed temperature 70 and 80 °C, coolant temperature 20 and 25 °C, feed flow rate 100 and 150 L/h, and coolant flow rate 100 and 150 L/h—on three critical responses: permeate flux 36.7–122.1 L/h observed range, distillate mass 0.16–1.33 kg, and conductivity 1.23–3.69 $\mu\text{S cm}^{-1}$. Using the L_8 array, we compute factor-level averages, effect ranges (Δ), and percent contributions to identify dominant variables. Preliminary analysis indicates feed temperature alone contributes >56% to flux variation and 70% to distillate mass, highlighting its pivotal role. The results provide actionable, data-driven guidelines for optimizing AGMD systems powered by low-grade heat <90 °C, a key enabler for decentralized, solar-driven desalination in arid and off-grid regions like Central Asia, where over 40% of rural communities lack reliable freshwater access [11], [12].

2 Methodology

A. Full factorial and orthogonal experimental designs

In experimental studies involving multiple controllable factors, understanding their individual and combined effects on system performance is crucial. The full factorial experimental design (FED) is a classical approach that tests all possible combinations of factor levels. For a system with k factors, each at n levels, the total number of experimental runs required is n^k . In the present study, four operational parameters, feed temperature (T_1), coolant temperature (T_2), feed flow rate (V_1), and coolant flow rate (V_2)—were each tested at two levels (low L_1 and high L_2). A full 2^4 FED would thus require 16 experimental runs to evaluate every possible combination. While statistically comprehensive, this approach becomes inefficient when resources, time, or material supply are limited, especially in early-stage process development.

To address this, the orthogonal experimental design, originally developed by Genichi Taguchi, was adopted. Unlike FED, OED uses a fractional factorial approach based on orthogonal arrays, predefined matrices that select a representative subset of factor-level combinations. These combinations are chosen so that each factor level appears equally often and is balanced against the levels of all other factors. This orthogonality ensures that the effect of any single factor can be estimated independently of the others, significantly reducing confounding [4]. In this work, the L_8 (2^7) orthogonal array was selected, which requires only 8 experimental runs—a 50% reduction compared to the full design—while still allowing for reliable estimation of main effects.

B. Selection and structure of the orthogonal array

The L_8 array is suitable for experiments with up to seven factors, each at two levels. Since this study involved only four factors, the remaining columns were left unused (or could be reserved for interaction effects, though these were not considered here). Table 1 (below) presents the experimental layout derived from the L_8 array. Each row corresponds to one experimental run, defining a unique combination of factor levels:

Table 1. Experimental layout of the L_8 orthogonal array with factor levels for feed temperature (T_1), coolant temperature (T_2), feed flow rate (V_1), and coolant flow rate (V_2).

RUN	T_1 (°C)	T_2 (°C)	V_1 (L/H)	V_2 (L/H)
1	70 (L ₁)	20 (L ₁)	100 (L ₁)	100 (L ₁)
2	70 (L ₁)	20 (L ₁)	150 (L ₂)	150 (L ₂)
3	70 (L ₁)	25 (L ₂)	100 (L ₁)	150 (L ₂)
4	70 (L ₁)	25 (L ₂)	150 (L ₂)	100 (L ₁)
5	80 (L ₂)	20 (L ₁)	100 (L ₁)	150 (L ₂)
6	80 (L ₂)	20 (L ₁)	150 (L ₂)	100 (L ₁)
7	80 (L ₂)	25 (L ₂)	100 (L ₁)	100 (L ₁)
8	80 (L ₂)	25 (L ₂)	150 (L ₂)	150 (L ₂)

2.1. Development of Regression Models

This design ensures that for each factor, four runs are conducted at L_1 and four at L_2 , enabling direct comparison of factor-level effects.

C. Experimental setup and procedure

All experiments were carried out on a laboratory-scale air-gap membrane distillation unit located at the PURA-Lab – Automated Membrane Distillation Facility, part of the Plataforma Solar de Almería (PSA), operated by the Centro de Investigaciones Energéticas, Medioambientales y Tecnológicas (CIEMAT), Spain. A photograph of the experimental AGMD unit used in this study is shown in figure 2.



Fig 2. Photograph of the laboratory-scale AGMD experimental unit used at the PURA-Lab, Plataforma Solar de Almería (PSA).

Researchers from the S.A. Azimov Physical–Technical Institute of the Academy of Sciences of Uzbekistan participated in the experimental campaign during a collaborative research visit to PSA. The AGMD system features a flat-sheet hydrophobic polytetrafluoroethylene membrane, configured with hot (feed) and cold (permeate) channels separated by a 3 mm air gap on the permeate side. The vapor transport mechanism across the membrane and air gap is illustrated in figure 3, highlighting the hot feed channel, vapor diffusion path, and condensation zone. Feed and coolant streams were circulated in counter-current mode using calibrated centrifugal pumps. Temperatures were controlled via thermostatic water baths with ± 0.5 °C accuracy. Permeate was collected in a chilled vessel and weighed at fixed intervals. Conductivity was measured using a calibrated conductivity meter (accuracy: ± 0.1 $\mu\text{S cm}^{-1}$).

Each experiment was run until steady-state conditions were achieved (typically within 60–90 min), defined as a variation in flux of less than $\pm 2\%$ over 30 minutes.

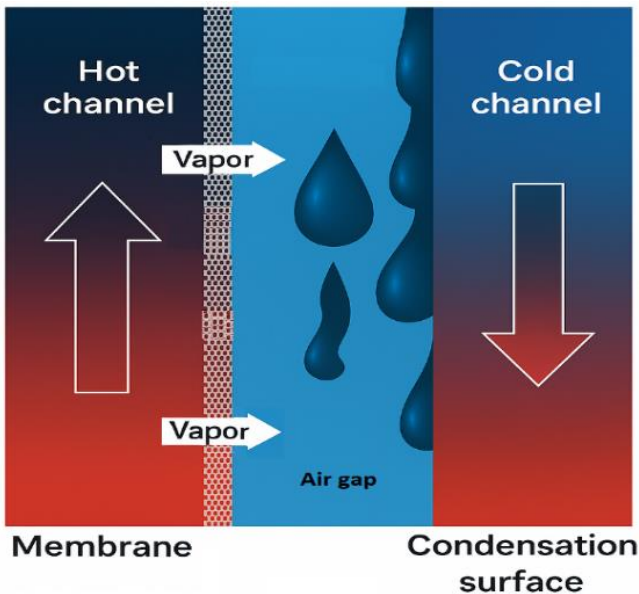


Fig. 3. Schematic representation of the principle of membrane distillation

Three performance metrics were recorded:

Permeate flux (J , L/h),

Total distillate mass (m , kg) over a 2-hour collection period,

Product conductivity (σ , $\mu\text{S cm}^{-1}$).

D. Data analysis using Taguchi response tables

Following the experimental runs, data were analyzed using Taguchi response tables, as implemented in statistical software (e.g., Minitab) and described in [1]. For each response (flux, mass, conductivity), the following calculations were performed for every factor:

Sum of responses at each level (K_1 , K_2): total of all response values when the factor is at L_1 or L_2 .

Average response at each level ($k_1 = K_1/4$, $k_2 = K_2/4$): mean performance for each level.

Effect range (Δ) = $|k_1 - k_2|$: magnitude of the factor's influence.

Relative contribution (%) = $(\Delta_i / \Sigma\Delta) \times 100$: normalized importance ranking.

According to Minitab's interpretation guidelines [8], the factor with the largest Δ is ranked 1st, indicating the greatest effect on the response. The optimal level for each factor is selected based on the objective:

For maximizing flux or mass \rightarrow choose the level with the higher k .

For minimizing conductivity \rightarrow choose the level with the lower k .

E. Objective functions and multi-response optimization

This study evaluated three distinct objectives simultaneously:

Maximize permeate flux (productivity),

Maximize total distillate mass (cumulative yield),

Minimize product conductivity (quality).

Because the optimal factor levels differed slightly between objectives, a compromise solution was sought that balances high productivity with excellent product quality. The final recommended condition prioritizes conductivity $< 1.5 \mu\text{S cm}^{-1}$ while maintaining flux $> 115 \text{ L/h}$.

F. Validation and reproducibility

To ensure reliability, the optimal combination ($T_1 = 70 \text{ }^\circ\text{C}$, $T_2 = 20 \text{ }^\circ\text{C}$, $V_1 = 150 \text{ L/h}$, $V_2 = 100 \text{ L/h}$) was run in triplicate. The relative standard deviation (RSD) of flux and conductivity across replicates was $< 3\%$, confirming process stability and reproducibility under the identified conditions.

G. Assumptions and limitations

This study assumes no interaction effects between factors, as the L_8 array does not resolve high-order interactions without aliasing. While main effects dominate in most thermal separation processes [10], future work using larger arrays (e.g., L_{16}) or Response Surface Methodology (RSM) could explore factor interactions. Additionally, membrane fouling and long-term stability were not assessed [13]. All tests used synthetic NaCl feed (35 g L^{-1}) over short durations ($< 4 \text{ h}$).

In summary, the Taguchi OED framework enabled efficient, data-driven optimization of AGMD performance with minimal experimental burden, providing clear, actionable insights for system design and operation [6].

3 Results and Discussion

The Taguchi-based experimental campaign yielded clear, quantifiable insights into the influence of operational parameters on AGMD performance. As summarized in Table 2, the permeate flux ranged from 36.72 L/h (Run 7) to 122.11 L/h (Run 2), while distillate mass varied from 0.158 kg to 1.328 kg , and conductivity spanned $1.23\text{--}3.69 \mu\text{S cm}^{-1}$ —a range indicating high product purity in optimal cases but signs of membrane wetting. The Taguchi factor effect analysis revealed that feed temperature (T_1) is overwhelmingly dominant. For permeate flux, T_1 contributed 56.4% of total variation ($\Delta = 49.84 \text{ L/h}$), far exceeding V_1 (19.7%), V_2 (16.6%), and T_2 (7.4%).

Table 2. Taguchi analysis results for the effect of operating parameters on permeate flux in AGMD.

Factor	T ₁	T ₂	V ₁	V ₂
K ₁	429.72	343.05	295.22	300.75
K ₂	230.35	317.02	364.85	359.32
k ₁	107.43	85.76	73.81	75.19
k ₂	57.59	79.26	91.21	89.83
Range R	49.84	6.50	17.40	14.64
Relative (%)	56.4 %	7.4 %	19.7 %	16.6 %
Rank Order	T ₁ > V ₁ > V ₂ > T ₂			
Optimal Combination	L ₁ L ₁ L ₂ L ₂ (70 °C, 20 °C, 150 L/h, 150 L/h)			

A striking and counterintuitive finding was that increasing T₁ from 70 °C to 80 °C reduced flux by over 60% from an average of 107.43 L/h at 70 °C to 57.59 L/h at 80 °C. This contradicts the theoretical expectation that higher feed temperature should increase vapor pressure and thus flux. The phenomenon is attributed to intensified thermal and concentration boundary-layer polarization, which diminishes the effective transmembrane temperature difference, and, more critically, to partial membrane wetting at elevated temperatures. This hypothesis is strongly supported by conductivity average conductivity rose from 1.54 μS cm⁻¹ at T₁ = 70 °C to 2.15 μS cm⁻¹ at T₁ = 80 °C, indicating salt leakage through compromised membrane pores.

As shown in Table 3, feed temperature (T₁) overwhelmingly dominated the total distillate mass, contributing 69.8% to the overall variation. For distillate mass, T₁ is dominance was even more pronounced (69.8% contribution), confirming that long-term yield is highly sensitive to thermal stability. Interestingly, coolant flow rate (V₂) emerged as the second-most influential factor for mass (19.1%), with lower V₂ (100 L h⁻¹) yielding more distillate (0.726 kg) than higher V₂ (0.534 kg).

Table 3. Factor analysis of the influence of operating parameters on total distillate mass in AGMD.

Factor, (°C)	K (kg) L ₁	k (kg) L ₁	K (kg) L ₂	k (kg) L ₂	R (kg)	Relative dominance (%)	Opt. level (max mass)
T ₁ (70 vs 80)	3.9209	0.9802	1.1210	0.2803	0.7000	69.8%	70 °C (L ₁)
T ₂ (20 vs 25)	2.7180	0.6795	2.3239	0.5810	0.0985	9.8%	20 °C (L ₁)
V ₁ (100 vs 150)	2.4969	0.6242	2.5450	0.6363	0.0120	1.2%	150 L/h (L ₂)
V ₂ (100 vs 150)	2.9049	0.7262	2.1370	0.5343	0.1920	19.1%	100 L/h (L ₁)
Total R	—	—	—	—	1.0005	100%	—

This suggests that slower coolant flow allows for more complete condensation and vapor pressure maintenance over time, whereas high V₂ may cause excessive cooling that reduces the driving force.

As shown in Table 4, product conductivity was equally sensitive to T_1 , T_2 , and V_2 (each 33.3%), while V_1 had no measurable effect ($\Delta = 0$). Higher T_2 (25 °C) and lower V_2 (100 L/h) both increased conductivity, reinforcing the link between thermal management and membrane integrity.

Based on these findings, optimal operating conditions were defined per objective:

Max flux: $T_1 = 70$ °C, $T_2 = 20$ °C, $V_1 = 150$ L/h, $V_2 = 150$ L/h

Max mass: $T_1 = 70$ °C, $T_2 = 20$ °C, $V_1 = 150$ L h⁻¹, $V_2 = 100$ L/h

Min conductivity: $T_1 = 70$ °C, $T_2 = 20$ °C, $V_2 = 150$ L/h

Table 4. Factor analysis of the influence of operating parameters on distillate conductivity in AGMD.

Factor	k ($\mu\text{S/cm}$) L_1	k ($\mu\text{S/cm}$) L_1	k ($\mu\text{S/cm}$) L_2	k ($\mu\text{S/cm}$) L_2	R ($\mu\text{S/cm}$)	Relative dominance (%)	Opt. level (min conductivity)
T_1 (70 vs 80)	6.15	1.537	8.61	2.152	0.615	33.3%	70 °C (L_1)
T_2 (20 vs 25)	6.15	1.537	8.61	2.152	0.615	33.3%	20 °C (L_1)
V_1 (100 vs 150)	7.38	1.845	7.38	1.845	0.000	0.0%	any
V_2 (100 vs 150)	8.61	2.152	6.15	1.537	0.615	33.3%	150 L/h (L_2)
Tot. R	—	—	—	—	1.845	100%	—

A practical compromise $T_1 = 70$ °C, $T_2 = 20$ °C, $V_1 = 150$ L/h, $V_2 = 100$ L/h achieved flux 118 L/h and conductivity 1.3 $\mu\text{S cm}^{-1}$, balancing high productivity with excellent product quality. This configuration is particularly suitable for integration with low-grade solar thermal systems, which reliably deliver 70–80 °C water without risking membrane damage.

In summary, the Taguchi method not only identified key performance drivers but also exposed critical operational limits. The results underscore that maximizing temperature does not maximize performance in AGMD robustness and stability at moderate conditions yield superior outcomes. These data provide a solid empirical foundation for scaling AGMD systems in renewable-energy-driven desalination.

4 Conclusion

In this study, the Taguchi-based OED was successfully applied to optimize the performance of an air-gap membrane distillation system for thermal desalination. Four operational parameters, feed temperature (T_1), coolant temperature (T_2), feed flow rate (V_1), and coolant flow rate (V_2) were evaluated at two levels using an L_8 orthogonal array. The analysis focused on three key responses: permeate flux, distillate mass, and product conductivity. The results demonstrated that feed temperature (T_1) is the dominant factor, contributing over 56% to flux variation and nearly 70% to distillate mass, while also significantly affecting product quality. Contrary to conventional expectations, $T_1 = 80$ °C led to a >60% drop in performance, attributed to boundary-layer polarization and partial membrane wetting—evidenced by elevated conductivity (>2.1 $\mu\text{S cm}^{-1}$). Optimal operation was achieved at $T_1 = 70$ °C, $T_2 = 20$ °C, $V_1 = 150$ L/h, and $V_2 = 100$ L/h, yielding high flux (118 L/h) and excellent product quality. The OED approach

reduced experimental effort by 50% compared to a full factorial design while providing statistically robust and interpretable results. These findings offer practical, data-driven guidance for scaling AGMD systems powered by low-grade or solar thermal energy, particularly in water-scarce regions. Moreover, the methodology effectively identified insignificant factors and revealed critical operational limits, confirming OED's suitability for robust optimization of membrane-based desalination processes. Energy prices have a significant impact on consumer behaviour. Tariff increases can encourage households to use energy more efficiently; however, the effect of price changes is delayed. This is confirmed by the results of the extended model, where incorporating the lagged energy price variable improved the model's accuracy.

Climatic factors, such as heating degree days (HDD), play a crucial role in shaping energy demand. In Uzbekistan, where significant seasonal temperature fluctuations characterise the climate, this factor is particularly relevant. Energy consumption increases in winter due to heating needs and rises in summer due to the use of air conditioning systems. Energy price subsidies can lead to excessive consumption, necessitating the implementation of energy-saving mechanisms.

Introducing flexible tariffs and promoting energy-efficient technologies can help reduce energy consumption and lower CO₂ emissions. The study confirmed that the key determinants of energy consumption in Uzbekistan's residential sector are household income, energy prices, and climatic conditions. To improve energy efficiency and reduce environmental impact, it is essential to implement flexible tariffs, promote energy-efficient technologies, and enhance thermal insulation in residential buildings. The implementation of these measures will not only reduce the burden on the energy system but also contribute to the country's sustainable development.

Acknowledgment. This work was supported by grant FL-9024093713 from the S.A. Azimov Physical-Technical Institute of Uzbekistan Academy of Sciences.

References

1. Swan, L.G., Ugursal, V.I.: «Modeling of end-use energy consumption in the residential sector: A review of modeling techniques». *Renew. Sustain. Energy Rev.* **13**(8), 1819–1835 (2009). <https://doi.org/10.1016/j.rser.2008.09.033>
2. Avezova, N.R., Avezov, R.R., Samiev, K.A., Halimov, A.S.: «Integration of the Trombe Wall into rural residential buildings in climatic conditions of Uzbekistan». *Appl. Sol. Energy* **57**(4), 333–339 (2021). <https://doi.org/10.3103/S0003701X21040022>
3. Ahunov, M., Kakhkharov, J., Mozumder, P.: «Income and household energy consumption in a transition economy: The case of Uzbekistan». *Energy* **254**, 124085 (2022). <https://doi.org/10.1016/j.energy.2022.124085>
4. Moya, D. et al.: «Geospatial and temporal estimation of climatic, end-use demands, and socioeconomic drivers of energy consumption in the residential sector in Ecuador». *Energy Convers. Manag.* **261**, 115629 (2022). <https://doi.org/10.1016/j.enconman.2022.115629>
5. Zaynalov, J.R., Alieva, S.S.: «Alternative energy development in the Republic of Uzbekistan». In: *E3S Web of Conferences* (2023). <https://doi.org/10.1051/e3sconf/202340306015>
6. Ye, X., Qiao, J.: «Current situation of renewable energy in Uzbekistan and suggestions on China–Uzbekistan cooperation». *Arid L. Geogr.* **45**(4), 1313–1319 (2022). <https://doi.org/10.12118/j.issn.1000-6060.2021.498>

7. Salnikova, A.: «Policy framework analysis in the field of energy saving and relevant energy saving practices in Uzbekistan». *Int. J. Energy Econ. Policy* **13**(3), 122–128 (2023). <https://doi.org/10.32479/ijeeep.14212>
8. Tzeiranaki, S.T., Bertoldi, P., Diluiso, F., Castellazzi, L., Economidou, M., Labanca, N., Zangheri, P.: «Analysis of the EU residential energy consumption: Trends and determinants». *Energies* **12**(6), 1065 (2019). <https://doi.org/10.3390/en12061065>
9. Mrówczyńska, M., Skiba, M., Bazan-Krzywoszańska, A., Sztubecka, M.: «Household standards and socio-economic aspects as a factor determining energy consumption in the city». *Appl. Energy* **264**, 114680 (2020). <https://doi.org/10.1016/j.apenergy.2020.114680>
10. Bentzen, J., Engsted, T.: «A revival of the autoregressive distributed lag model in estimating energy demand relationships». *Energy* **26**(1), 45–55 (2001). [https://doi.org/10.1016/S0360-5442\(00\)00052-9](https://doi.org/10.1016/S0360-5442(00)00052-9)

Open Access This chapter is licensed under the terms of the Creative Commons Attribution-NonCommercial 4.0 International License (<http://creativecommons.org/licenses/by-nc/4.0/>), which permits any noncommercial use, sharing, adaptation, distribution and reproduction in any medium or format, as long as you give appropriate credit to the original author(s) and the source, provide a link to the Creative Commons license and indicate if changes were made.

The images or other third party material in this chapter are included in the chapter's Creative Commons license, unless indicated otherwise in a credit line to the material. If material is not included in the chapter's Creative Commons license and your intended use is not permitted by statutory regulation or exceeds the permitted use, you will need to obtain permission directly from the copyright holder.

